Ionic Conductivity of $Ce_{0.91}Ca_{0.09}O_{2-\delta}$ as an Electrolyte for Intermediate Temperature Solid Oxide Fuel Cells

Momin Naeemakhtar and Manjanna J.*
Department of Chemistry, Rani Channamma University, Belagavi-591156, Karnataka, INDIA
*jmanjanna@rediffmail.com

Abstract
*The search for new cost-effective electrolyte materials for IT-SOFC towards its mass scale commercialization has gained momentum in recent years. The Ca- doped ceria having composition $Ce_{0.91}Ca_{0.09}O_{2-\delta}$ was prepared using the facile conventional solid-state method. The structural and electrical properties of low sintered ceramic samples have been characterized by X-ray diffraction (*XRD*),* UV–*VIS diffuse reflectance* spectroscopy *(*DRS*) and A.C. impedance technique respectively. The oxide ion conductivity was measured between the temperatures 573 K−973 K in air. The obtained results showed that total conductivity is mainly dependent on the grain boundary effect.*

The nanocrystalline $Ce_{0.91}Ca_{0.09}O_{2-\delta}$ exhibited the high total ionic conductivity of 7.36 $\times 10^{-3}$ S cm^{-1} at 973 K with a lower activation energy of 0.96 eV. The obtained results highlight the use of cost-effective dopant in ceria lattice to develop commercially viable electrolyte materials for IT-SOFC.

Keywords: IT-SOFC, Electrolyte, $Ce_{0.91}Ca_{0.09}O_{2-\delta}$, A.C. impedance, Ionic conductivity.

Introduction

Solid oxide fuel cell (SOFC) has emerged as an energy conversion device in achieving high electrical efficiency with regeneration and simultaneously offering an incredible guarantee of delivering significant environmental benefits in fuel flexibility with clean and efficient electric power generation[24,28]. Lowering the operating temperature to intermediate temperature (IT) (Ca: 873 K − 1073 K) in the current scenario is an emerging trend towards its commercialization. It thus instigated the research community for developing low-temperature oxygen ion or proton conductive materials for SOFC applications[9]. An electrolyte being an oxide ion/proton conductor plays a vital role in SOFC[14]. It is sandwiched between cathode and anode. The ions get transported through it by the hopping mechanism[5]. In an electrochemical reaction, the conduction of oxide ion/proton occurs from the cathode to anode through the electrolyte and reacts with hydrocarbon to form H_2O[42]. The high ionic and negligible electronic conductivity, permanence in redox atmosphere, good mechanical properties are the main features for selecting SOFC electrolyte materials[15].

**** Author for Correspondence***

Numerous materials for oxide-ion electrolytes were identified like zirconia and ceria-based oxides having fluorite structures, stabilized δ–Bi_2O_3, Pyrochlores, oxygen-deficient Perovskites $La_{1-x}Sr_xGa_{1-y}Mg_yO_{3-\delta}$ (LSGM) and bismuth metal vanadium oxide (BIMEVOX) etc. Still all fell short at an operating temperature below 800 ^oC[26].

At the intermediate operating temperature (Ca: 873 K − 1073 K), the doped ceria samples showed ionic conductivity one order higher than the yttria-stabilized zirconia (YSZ) system[38]. The high conductivity is attributed to a large ionic radius of Ce^{4+} (0.87 Å) compared to Zr^{4+} (0.72 Å) creating a more open structure to ease the conduction for oxide ions. Unlike zirconia, the ceria possesses the natural fluorite structure from room temperature to its melting point at 2673 K where phase transition occurs at different temperatures[4]. Therefore, in doped ceria ceramics, doping is the only cause for the formation of vacancies. The common dopants used in ceria were Gd^{3+}, Sm^{3+} and y^{3+}. The Gd^{3+} is the most commonly used due to their lowest ionic radius mismatch[10].

Doping of Gd^{3+} to Ce^{4+} lattice can present the smallest stress and yield high ionic conductivity with lower activation energy for the O^{2-} conduction[19]. The 10 mol % Gd doped-Ceria [$Ce_{0.9}Gd_{0.1}O_{1.95}$] composition was promising for IT-SOFC applications since it was found to deliver high ionic conductivity 773 K[22]. Gadolinium doped ceria (GDC), apart from high ionic conductivity is also compatible with the LSCF cathode materials[12]. The chemical reaction of GDC with electrodes was found to be negligible[33].

But at high temperatures, some issue with their electronic conduction arises under a reduced atmosphere at anode interface when Ce^{4+} reduces to Ce^{3+}. This electronic conductivity reduces the open-circuit voltage and enhances the fuel consumption, thereby affecting the cell's performance[6,36]. The Gd- and Sm-doped ceria are considered as potential electrolytes for IT-SOFC applications[02]. But the cost of these dopants for 10−20 mol % is highly expensive[39].

Thus the development of new commercially viable ceria-based electrolyte materials is the need of the hour. The abundant and high economical calcium doped ceria materials showed high ionic conductivity comparable to other rare earth doped creia materials[31]. Thus, the Ca (r_i =1.12 Å) doped with ceria (r_i =1.11 Å) has been investigated at large[23]. The calcium (Ca^{2+}) doped ceria emerged as a cost-effective electrolyte for IT-SOFC.

Calcium doping creates high oxygen vacancies and is regarded as suitable oxygen storage material. Yamashita et

al[40] and Banerjee et al[7] reported high conductivity in the order of 10^{-3} S cm^{-1} and 1.29×10^{-2} S cm^{-1} at 873 K for $Ce_{0.9}Ca_{0.1}O_{2-\delta}$ and $Ce_{0.8}Ca_{0.2}O_{2-\delta}$ compositions prepared by the auto combustion method respectively. Thus from the commercial viability prospect in the present work, the Ca^{2+} – doped ceria having composition $Ce_{0.91}Ca_{0.09}O_{2-\delta}$ which was not reported, has been prepared through facile and conventional solid-state method[43]. The A.C. impedance analysis was carried between the temperature range from 623 – 973 K in air. This work intends to explore new low-cost Ca-doped ceria ceramics for IT-SOFC applications.

Material and Methods

The $Ce_{0.91}Ca_{0.09}O_{2-\delta}$ has been synthesized from the conventional solid-state method. The precursors ceric oxide (CeO_2) and calcium acetate hydrate [$Ca(C_2H_3O_2)_2.xH_2O$] of AR grades were purchased from SDFCL Limited, Mumbai, India. A stoichiometric amount of precursors was mixed with isopropyl alcohol in agate mortar-pestle for an hour and heated to 673 K for 6 h. The mixture was again ground and calcined at 1273 K for about 6 h to get the final product. For A.C. impedance measurement, the obtained powder was pelletized (dimension of (10 ϕ× 2) mm) at 5 MPa with 4 wt. % of polyvinyl alcohol (as a binder) and sintered at 1473 K in the air for about 4 h.

Characterization: The X-ray diffraction analysis (XRD) [Rigaku MiniFlex 600 powder with Cu Ka radiation (λ = 0.154 nm)] was used to study the crystal structure of $Ce_{0.91}Ca_{0.09}O_{2-\delta}$ sample. The Profex 4.3.2 software was used for Rietveld refinement. Relative density was calculated using the Archimedes method. The diffused reflectance spectral (DR-UV-Vis) analysis of the $Ce_{0.91}Ca_{0.09}O_{2-\delta}$ was performed by using Jasco spectrophotometer V-77. For electrical connection, the silver paste was applied on both sides of the pellet and baked at 873 K for 1 h. The CH Instrument (Inc CHI604D USA) was used to record the Nyquist plots at different temperatures between 623 – 973 K in the frequency range of 1 – 10 MHz with an A.C. signal of 10 mA. The obtained data were fitted to the corresponding equivalent circuits [R(QR)(QR)] using the ZSimpWin software. Total oxide ion conductivity (σ) was calculated using the eq. (1):

$$\sigma = t / RA \quad (1)$$

where t is the thickness of the pellet, A is the area of cross-section and R is the total resistance.

Results and Discussion

Figure 1 shows the XRD patterns of CeO_2 and $Ce_{0.91}Ca_{0.09}O_{2-\delta}$ pellets sintered at 1473 K. It has been observed that the sample $Ce_{0.91}Ca_{0.09}O_{2-\delta}$ exhibited the same XRD pattern as CeO_2 matching with ICDD card No 34-0394. The diffraction peaks were indexed as per standard fluorite structure with space group Fm3m. The no diffraction peaks corresponding to CaO or other impurities were observed indicating the formation of a single-phase solid solution. The XRD analysis of the $Ce_{0.91}Ca_{0.09}O_{2-\delta}$ showed a typical lattice structure aligned with the reported lattice parameter of 5.411 Å for pure CeO_2 as indicated in the ICDD card and those obtained from Rietveld refinement. The sharp peaks in the XRD patterns of pellets indicate larger crystallite size due to high-temperature sintering[13].

The replacement of smaller ionic radii of Ce (r_i = 0.97 Å) by a larger ionic radius Ca (r_i =1.05 Å) creates the incongruity between the ions generating the oxygen vacancies in the CeO_2 lattice. The oxygen vacancies cause the lattice strain to retain the charge equilibrium state which resulted in expansion of unit cell[20].

The generated strain at lattice may get localized at a sub-grain and sub-domain level near the grain boundaries. This attributed to the decrease in crystallite size in doped sample ($Ce_{0.91}Ca_{0.09}O_{2-\delta}$)[30]. The crystallite sizes (D) were computed from the preferential plane width (111) using Scherrer's equation. The obtained crystallite sizes for the CeO_2 and $Ce_{0.91}Ca_{0.09}O_{2-\delta}$ pellets were 88 nm and 82 nm respectively.

The dislocation density (δ) gives information about the number of defects in the crystal and calculated from eq. (2).

$$\delta = \frac{1}{D^2} \quad (2)$$

where D is the average crystallite size.

The dislocation density as a function of dopant concentration revealed an excellent crystalline nature of the compound[35]. The theoretical surface areas were calculated by using eq. (3).

$$S = \frac{6}{DX\rho} \quad (3)$$

where D is the average crystallite size and ρ is the X-ray density. The obtained values of dislocation density and specific surface area for CeO_2 and $Ce_{0.91}Ca_{0.09}O_{2-\delta}$ samples were listed in table 1.

The XRD pattern of $Ce_{0.91}Ca_{0.09}O_{2-\delta}$ obtained after Rietveld refinement is shown in figure 2. The refined parameters (R-factors) which determine goodness of fit (GoF) for peak shape, position, structure and background were shown in table 2. The lower values of R_p and R_{wp} indicate the goodness of fit. The difference between observed and calculated patterns was found to be negligible.

The diffuse reflectance (DR) UV-visible absorption spectra of the CeO_2 and $Ce_{0.91}Ca_{0.09}O_{2-\delta}$ are shown in figure 3. The peaks appeared around 291 nm in the ultraviolet absorption region attributed to the charge transition from the O 2p band to Ce 4f band and the formation of excess oxygen vacancies[25]. This red-shift is due to the interfacial polaron effect emerging from electron−phonon interaction[4].

The Kubelka–Munk equation was used to obtain the optical band gap and it was determined from $[F(R)h\vartheta]^{1/2}$ against E_g. The obtained plots are shown in figure 4. The decreased band gap energy obtained for $Ce_{0.91}Ca_{0.09}O_{2-\delta}$ (2.81 eV) compared to CeO_2 (2.97 eV) which was confirmed the substitution of Ca^{2+} ions by Ce^{4+} from CeO_2 lattice[18]. Thus, during doping, Ca^{2+} ions are generated at the ground and excited f - energy state in the CeO_2 band. Therefore, energy states of Ca^{2+} will trap many excited electrons coming from the O2–2p level and causes the reduction in band-gap energy[1]. Therefore, the band-gap energy is inversely related to the ionic conductivity.

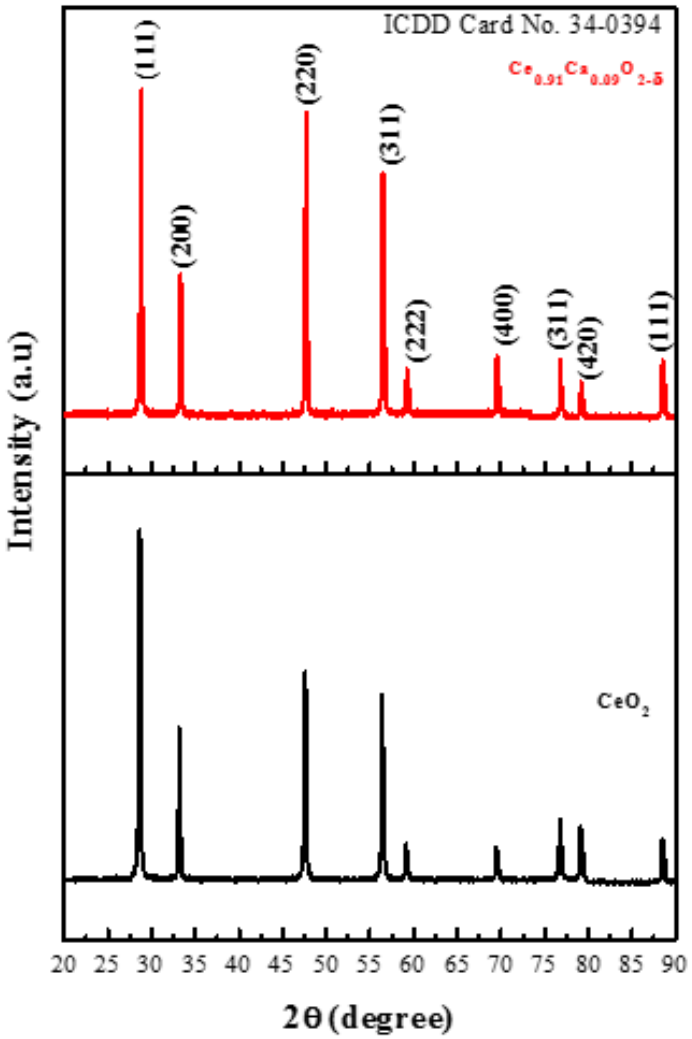

Figure 1: XRD pattern of CeO_2 and $Ce_{0.91}Ca_{0.09}O_{2-\delta}$ Pellets and sintered at 1473 K

Table 1
Structural characteristics of CeO_2 and $Ce_{0.91}Ca_{0.09}O_{2-\delta}$ samples.

Samples	Average crystallite size, D (nm)	Dislocation Density, δ (line/m²×10⁻¹⁵)	Specific surface area (m²/g)	Bandgap, *Eg* (eV)	Relative density (%)
CeO_2	88	0.1291	9.45	2.97	93
$Ce_{0.91}Ca_{0.09}O_{2-\delta}$	82	0.1487	10.18	2.81	95

Table 2
Rietveld refinement parameters of CeO_2 and $Ce_{0.91}Ca_{0.09}O_{2-\delta}$ samples.

Samples	Lattice constant a = b = c (Å)	Volume (Å)³	Agreement factors		
			R_P	R_{wp}	GoF
CeO_2	5.401	158.2	5.82	13.20	2.26
$Ce_{0.91}Ca_{0.09}O_{2-\delta}$	5.415	158.8	6.99	16.29	2.33

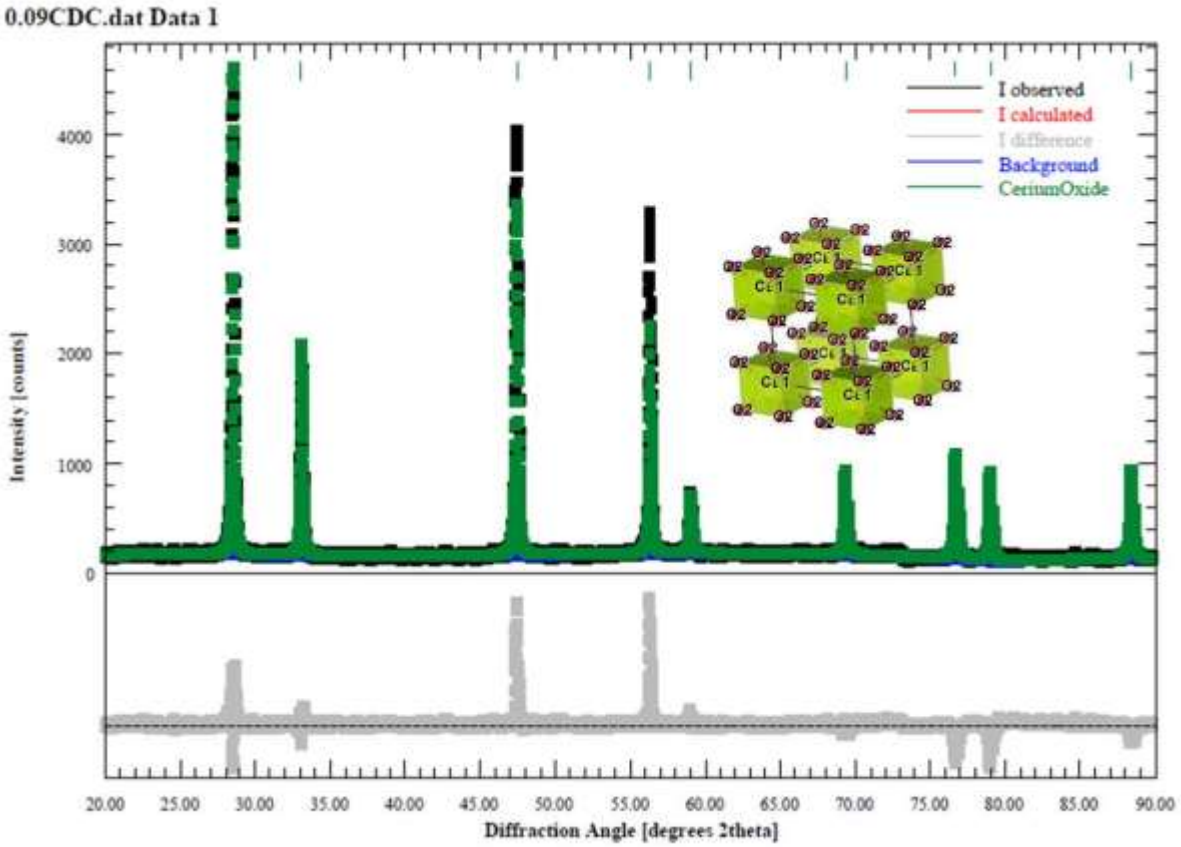

Figure 2: XRD patterns after Rietveld refinement of $Ce_{0.91}Ca_{0.09}O_{2-\delta}$ sample

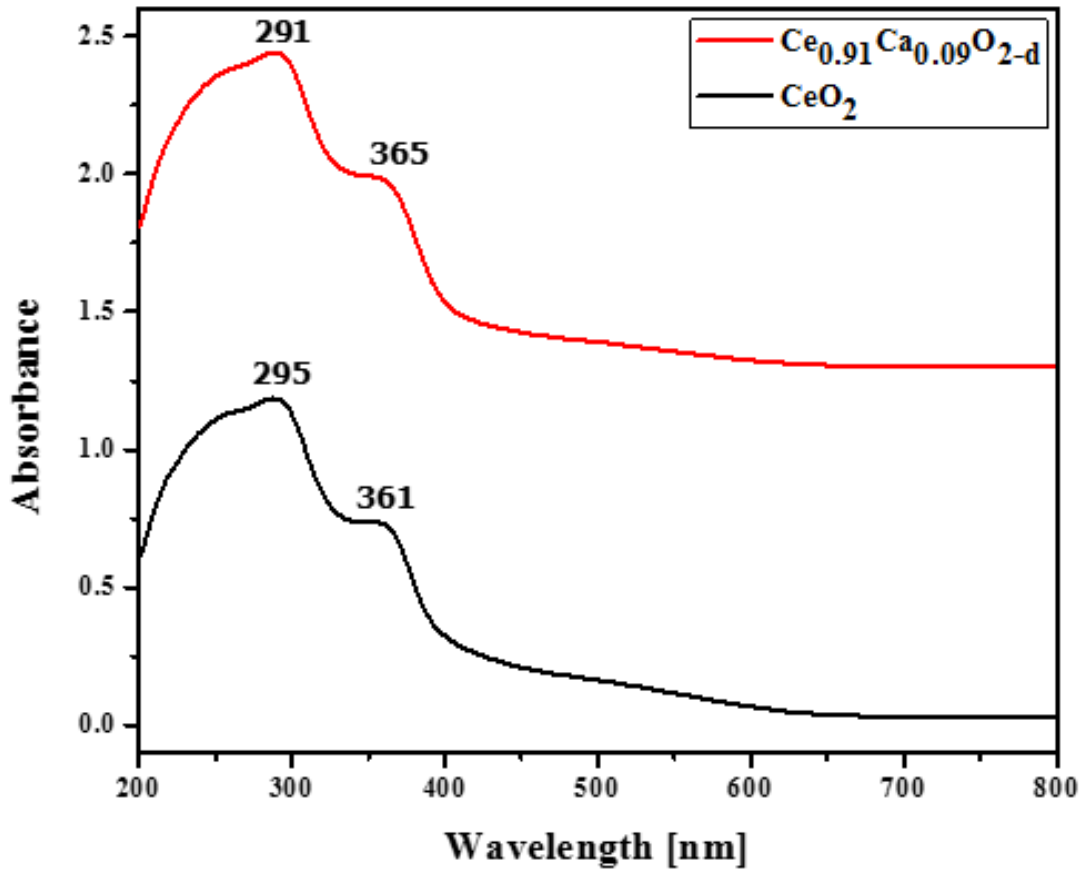

Figure 3: UV-Visible diffuse reflectance spectra of CeO_2 and $Ce_{0.91}Ca_{0.09}O_{2-\delta}$ samples

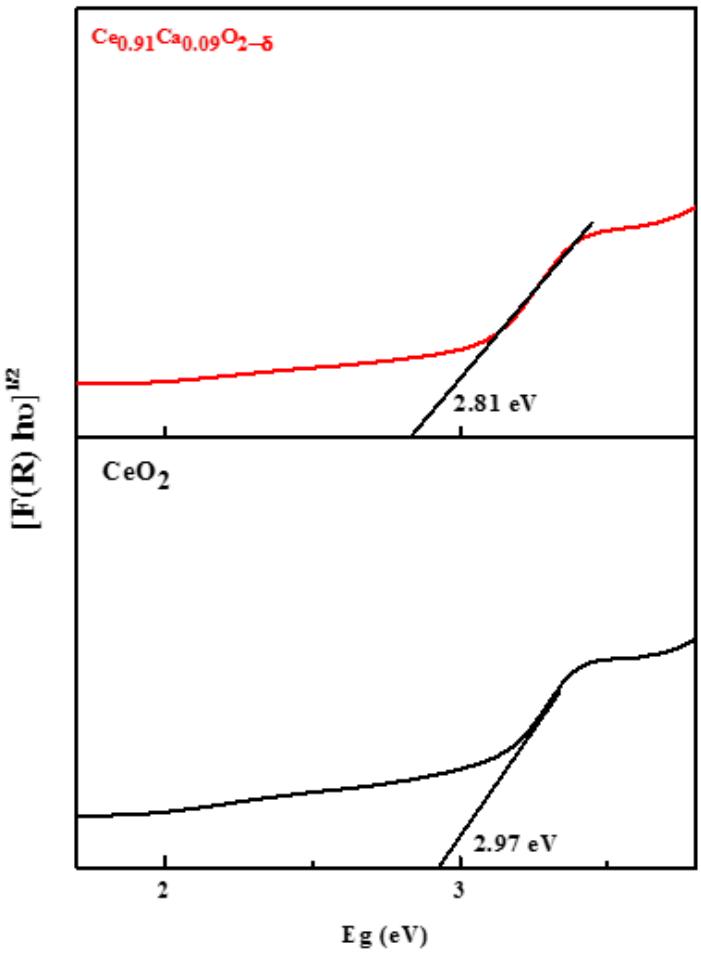

Figure 4: Kubelka–Munk plots of CeO_2 and $Ce_{0.91}Ca_{0.09}O_{2-\delta}$ samples

Figure 5 shows the Nyquist plots obtained from impedance measurement in the air between temperatures 623 – 973 K as a function of frequency. The typical A.C. impedance spectrum consists of different contributions to grain, grain boundary (GB) and electrode behaviour. At a constant temperature, all arcs will not appear due to different relaxation time constants for individual polarization of conductors. Therefore, at high temperature, the only arc belongs to electrode behaviour emerged. An equivalent electrical circuit model [R(QR)(QR)] was employed to distinguish these grain, GB and electrode behavioral arcs as shown in the inset of fig. 5.

The equivalent circuit consists of the grain resistance (R_g) and two RC circuits in series for GB (R_{gb}) and the other for electrode polarization (R_e). A constant phase element (CPE = Q) is applied instead of a capacitor. This constant phase element is equivalent to the distribution of the capacitor in parallel. The element R_g, $R_{gb}\|Q$ represents the ionic conductivity through grain and grain boundary[34,37]. The total resistance of the electrolyte is calculated by using the eq. (4):

$$R_t = R_g + R_{gb} \quad (4)$$

where R_g and R_{gb} are grain and GB resistance respectively. The total conductivity is obtained by using eq. (1).

Temperature dependency on conductivity for $Ce_{0.91}Ca_{0.09}O_{2-\delta}$ was shown by using Arrhenius eq. (5):

$$\sigma T = A_o \exp^{\left(\frac{-E_a}{KT}\right)} \quad (5)$$

where σ, A_o, T, E_a and K are conductivity, pre-exponential constant, temperature, activation energy and Boltzmann constant. Figure 6 shows the Arrhenius plots for the grain, GB and total conductivity of $Ce_{0.91}Ca_{0.09}O_{2-\delta}$ sample. The obtained activation energies for grain, GB and total conduction were enlisted in table 3.

From the obtained results, it has been observed that conductivity linearly varies with temperature. The major contribution to the total conductivity was from grain (bulk) conductivity[41]. The doping of Ca^{2+} to CeO_2 lattice has significantly enhanced ionic conductivity compared to CeO_2[29].

The improved performance of $Ce_{0.91}Ca_{0.09}O_{2-\delta}$ is attributed to the enhancement in charge carriers arising due to the formation of oxygen vacancies resulting from doping. The expansion of the crystal structure during Ca^{2+} doping could improve the mobility of the oxygen ions and thus resulted in high ionic conductivity[32].

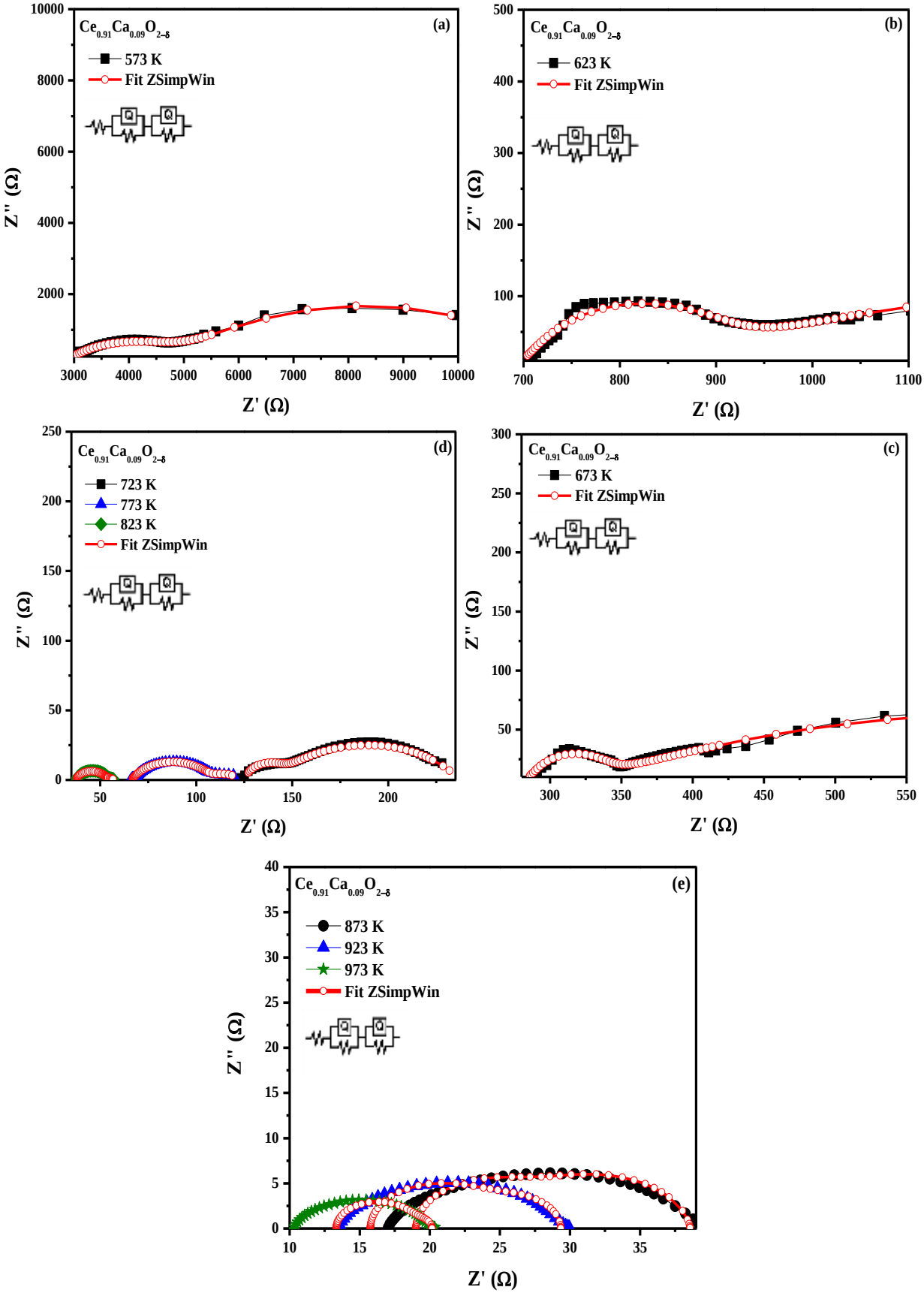

Figure 5: Nyquist plots of $Ce_{0.91}Ca_{0.09}O_{2-\delta}$ measured at (a) 573 K, (b) 623 K, (c) 673 K, (d) 723 – 823 K and (e) 873 – 973 K temperatures

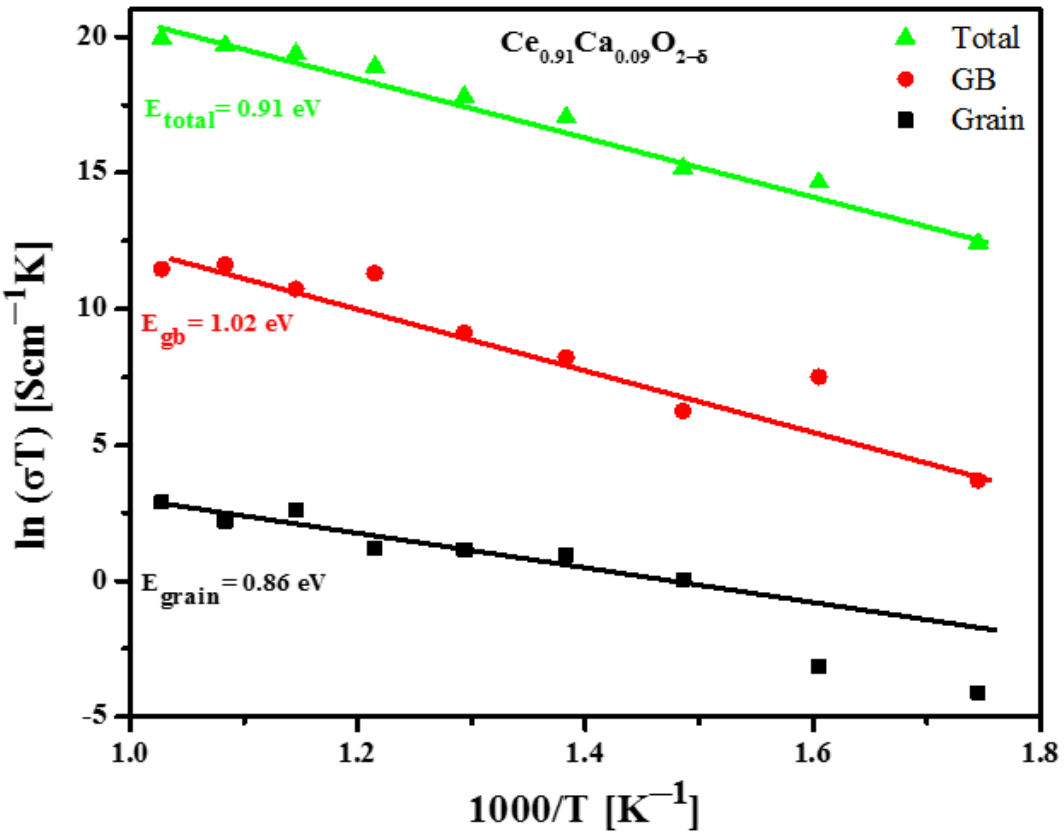

Figure 6: Arrhenius plots for total, grain boundary and grain conductivity of $Ce_{0.91}Ca_{0.09}O_{2-\delta}$.

Table 3
The grain, GB, total conductivity and activation energy of $Ce_{0.91}Ca_{0.09}O_{2-\delta}$.

	Conductivity (σ) [Scm^{-1}]		
Temperature (K)	**Grain**	**GB**	**Total**
573	2.86×10^{-5}	8.71×10^{-6}	6.67×10^{-6}
623	6.81×10^{-5}	3.64×10^{-4}	5.73×10^{-5}
673	1.56×10^{-3}	9.46×10^{-5}	8.92×10^{-5}
723	3.62×10^{-3}	6.39×10^{-4}	5.43×10^{-4}
773	4.06×10^{-3}	1.47×10^{-3}	1.08×10^{-3}
823	4.08×10^{-3}	1.23×10^{-2}	3.06×10^{-3}
873	1.52×10^{-2}	6.56×10^{-3}	4.59×10^{-3}
923	9.73×10^{-3}	1.52×10^{-2}	5.93×10^{-3}
973	1.85×10^{-2}	1.22×10^{-2}	7.36×10^{-3}
Activation Energy E_a, (eV)	0.86	1.02	0.91

The calcium was used as a sintering aid for ceria-based electrolytes and therefore doping yields high dense ceramic at a lower sintering temperature of 1473 K[8].

It has been observed that the high grain, GB and total conductivity of 1.85×10^{-2}, 1.22×10^{-2} and 7.36×10^{-3} S cm^{-1} at 973 K were obtained with a lower activation energy of 0.86, 1.02 and 0.96 eV respectively for $Ce_{0.91}Ca_{0.09}O_{2-\delta}$ sample. The obtained results of $Ce_{0.91}Ca_{0.09}O_{2-\delta}$ were compared with the reported conductivity of 8.01×10^{-3}, 6.31×10^{-3} and 1.13×10^{-3} S cm^{-1} at 973 K for $Ce_{0.9}Ca_{0.1}O_{2-\delta}$ sample prepared from combustion method using citric acid, glycine and urea as fuel respectively by Ong et al.[27]

Similarly, obtained results for the $Ce_{0.91}Ca_{0.09}O_{2-\delta}$ at 973 K were compared with the other potential electrolyte materials like $Ce_{0.8}Sm_{0.2}O_{2-\delta}$ (7.7×10^{-2} S cm^{-1} at 973 K)[16], $Ce_{0.9}Gd_{0.1}O_{2-\delta}$ (3.6×10^{-2} S cm^{-1} at 973 K)[21], $Ce_{0.9}La_{0.1}O_{2-\delta}$ (5.9×10^{-3} S cm^{-1} at 873 K)[11] and $Ce_{0.85}La_{0.15}O_{2-\delta}$ (9.4×10^{-4} S cm^{-1} at 873 K)[17].

Therefore, cost-effective Ca^{2+}-doped ceria ($Ce_{0.91}Ca_{0.09}O_{2-\delta}$) which are capable of delivering competitive results over potential electrolyte materials could reduce the cost for IT-SOFC. Thus, the nanocrystalline $Ce_{0.91}Ca_{0.09}O_{2-\delta}$ is regarded as potential electrolyte materials for IT-SOFC.

Conclusion

The $Ce_{0.91}Ca_{0.09}O_{2-\delta}$ has been successfully synthesized by the cost-effective conventional solid-state method. The XRD and Rietveld refinement confirm the formation of a single-phase solid solution. The particles have a crystallite size below 100 nm. The DRS-UV-Vis confirmed the red-shift of the peak in the ultraviolet absorption region due to the interfacial polaron effect emerging from electron–phonon interaction. The band gap for $Ce_{0.91}Ca_{0.09}O_{2-\delta}$ is lower than CeO_2 and thus confirmed the substitution of Ca^{2+} ions by Ce^{4+} into CeO_2 lattices, thereby generating excessive oxygen vacancies.

The A.C. impedance analyses were carried between temperatures 573 – 973 K. The $Ce_{0.91}Ca_{0.09}O_{2-\delta}$ exhibited the high ionic conductivity for grain (1.85×10^{-2} S cm^{-2}) and total (7.36×10^{-3} S cm^{-3}) at 973 K. The lower activation energy obtained for grain, GB and total conduction was 0.86, 1.02 and 0.96 eV respectively. Thus, the nanocrystalline $Ce_{0.91}Ca_{0.09}O_{2-\delta}$ may be regarded as cost-effective potential electrolyte for IT-SOFC.

Acknowledgement

Authors greatly acknowledge the financial support from (i) BRNS/ DAE, Govt. of India [37 (2)/14/20/2015/BRNS] (ii) DST-FIST, Govt. of India [SR/FST/CSI-273/2016] and (iii) Surface Engineering Division (SED), CSIR-National Aerospace Laboratories, Bengaluru-560017, India.

References

1. Abbas F., Jan T., Iqbal J., Ahmad I., Naqvi M.S.H. and Malik M., Facile synthesis of ferromagnetic Ni doped CeO_2 nanoparticles with enhanced anticancer activity, *Applied Surface Science*, **357**, 931–936 **(2015)**

2. Ali A., Raza R., Kaleem Ullah M., Rafique A., Wang B. and Zhu, B., Alkaline earth metal and samarium co-doped ceria as efficient electrolytes, *Applied Physics Letters*, **112(4)**, 043902−5 **(2018)**

3. Amarsingh Bhabu K., Theerthagiri J., Madhavan J., Balu T. and Rajasekaran T.R., Superior oxide ion conductivity of novel acceptor doped cerium oxide electrolytes for intermediate-temperature solid oxide fuel cell applications, *The Journal of Physical Chemistry C*, **120(33)**, 18452–18461 **(2016)**

4. Amarsingh Bhabu K., Theerthagiri J., Madhavan J., Balu T., Muralidharan G. and Rajasekaran T.R., Cubic fluorite phase of samarium doped cerium oxide $(CeO_2)_{0.96}Sm_{0.04}$ for solid oxide fuel cell electrolyte, *Journal of Materials Science: Materials in Electronics*, **27(2)**, 1566–1573 **(2016)**

5. Anjaneya K.C., Nayaka G.P., Manjanna J., Govindaraj G. and Ganesha K.N., Studies on structural, morphological and electrical properties of $Ce_{0.8}Ln_{0.2}O_{2-\delta}$, (Ln = Y^{3+}, Gd^{3+}, Sm^{3+}, Nd^{3+} and La^{3+}) solid solutions prepared by citrate complexation method, *Journal of Alloys and Compounds*, **585**, 594–601**(2014)**

6. Anjaneya K.C., Rare earth ion doped ceria as electrolytes for solid oxide fuel cell, *Advanced Materials Letters*, **7(9)**, 743–747 **(2016)**

7. Banerjee S. and Devi P.S., Understanding the effect of calcium on the properties of ceria prepared by a mixed fuel process, *Solid State Ionics*, **179(17–18)**, 661–669 **(2008)**

8. Banerjee S., Devi P.S., Topwal D., Mandal S. and Menon K., Enhanced ionic conductivity in $Ce_{0.8}Sm_{0.2}O_{1.9}$: unique effect of calcium Co-doping, *Advanced Functional Materials*, **17(15)**, 2847–2854 **(2007)**

9. Biswas M. and Sadanala K.C., Electrolyte materials for solid oxide fuel cell, *Journal of Powder Metallurgy & Mining*, **2**, 1–6 **(2013)**

10. Campbell C.T., Chemistry: oxygen vacancies and catalysis on ceria surfaces, *Science*, **309(5735)**, 713–714 **(2005)**

11. Dikmen S., Shuk P. and Greenblatt M., Hydrothermal synthesis and properties of $Ce_{1-x}La_xO_{2-\delta}$ solid solutions, *Solid State Ionics*, **126(1)**, 89–95 **(1999)**

12. Eguchi K., Setoguchi T., Inoue T. and Arai H., Electrical properties of ceria-based oxides and their application to solid oxide fuel cells, *Solid State Ionics*, **52(1–3)**, 165–172 **(1992)**

13. Feng B., Sugiyama I., Hojo H., Ohta H., Shibata N. and Ikuhara Y., Atomic structures and oxygen dynamics of CeO_2 grain boundaries, *Scientific Reports*, **6**, 1–7 **(2016)**

14. Goodenough J.B., Oxide-ion electrolytes, *Annual Review of Materials Research*, **33(1)**, 91–128 **(2003)**

15. Jacobson A.J., Materials for solid oxide fuel cells, *Chemistry of Materials*, **22(3)**, 660–674 **(2010)**

16. Jaiswal N., Kumar D., Upadhyay S. and Parkash O., Ceria co-doped with calcium (Ca) and strontium (Sr): A potential candidate as a solid electrolyte for intermediate temperature solid oxide fuel cells, *Ionics*, **20(1)**, 45–54 **(2014)**

17. Jaiswal N., Upadhyay S., Kumar D. and Parkash O., Ionic conductivity investigation in lanthanum (La) and strontium (Sr) co-doped ceria system, *Journal of Power Sources*, **222**, 230–236 **(2013)**

18. Karl C.M. et al, Synthesis and enhanced electrochemical properties of Sm:CeO_2 nanostructure by hydrothermal route, *Materials Letters*, **113**, 170–173 **(2013)**

19. Knoblauch N., Dörrer L., Fielitz P., Schmücker M. and Borchardt G., Surface controlled reduction kinetics of nominally undoped polycrystalline CeO_2, *Physical Chemistry Chemical Physics*, **17(8)**, 5849–5860 **(2015)**

20. Kurian M. and Kunjachan C., Investigation of size dependency on lattice strain of nanoceria particles synthesised by wet chemical methods, *International Nano Letters*, **4(4)**, 73–80 **(2014)**

21. Liu A.Z., Wang J.X., He C.R., Miao H., Zhang Y. and Wang W.G., Synthesis and characterization of $Gd_{0.1}Ce_{0.9}O_{1.95}$ nanopowder via an acetic-acrylic method, *Ceramic International*, **39(6)**, 6229–6235 **(2013)**

22. Loche D., Morgan L.M., Casu A., Mountjoy G., O'Regan C., Corrias A. and Falqui A., Determining the maximum lanthanum

incorporation in the fluorite structure of La-doped ceria nanocubes for enhanced redox ability, *RSC Advances*, **9(12)**, 6745–6751 **(2019)**

23. Ma Y., Wang X., Khalifa H.A., Zhu B. and Muhammed M., Enhanced ionic conductivity in calcium doped ceria - Carbonate electrolyte: A composite effect, *International Journal of Hydrogen Energy*, **37(24)**, 19401–19406 **(2012)**

24. Mahato N., Banerjee A., Gupta A., Omar S. and Balani K., Progress in material selection for solid oxide fuel cell technology: A review, *Progress in Materials Science*, **72**, 141–337 **(2015)**

25. Manoharan D. and Vishista K., Optical properties of nano-crystalline cerium dioxide synthesized by single step aqueous citrate-nitrate gel combustion method, *Asian Journal of Chemistry*, **25(16)**, 9045–9049 **(2013)**

26. Momin N., Manjanna J., Rane K.S., Kumar A., Senthilkumar S. and Aruna S.T., Structural and ionic conductivity of Cu-doped titania ($Ti_{0.95}Cu_{0.05}O_{2-\delta}$) for high temperature energy devices, *Ceramics International*, **47(7)**, 10284–10290 **(2021)**

27. Ong P.S., Tan Y.P., Taufiq-Yap Y.H. and Zainal Z., Improved sinterability and conductivity enhancement of 10-mol% calcium-doped ceria using different fuel-aided combustion reactions and its structural characterization, *Materials Science Engineering B: Solid-State Materials for Advanced Technology*, **185(1)**, 26–36 **(2014)**

28. Orera A. and Slater P.R., New chemical systems for solid oxide fuel cells, *Chemistry of Materials*, **22(3)**, 675–690 **(2010)**

29. Parkash O., Singh N., Singh N.K. and Kumar D., Preparation and characterization of ceria co-doped with Ca and Mg, *Solid State Ionics*, **212**, 100–105 **(2012)**

30. Patsalas P., Logothetidis S., Sygellou L. and Kennou S., Structure-dependent electronic properties of nanocrystalline cerium oxide films, *Physical Review B - Condensed Matter and Materials Physics*, **68(11)**, 1–13 **(2003)**

31. Raza R., Qin H., Fan L., Takeda K., Mizuhata M. and Zhu B., Electrochemical study on co-doped ceria-carbonate composite electrolyte, *Journal of Power Sources*, **201**, 121–127 **(2012)**

32. Song H. and Ozkan U.S., Changing the oxygen mobility in Co/ceria catalysts by Ca incorporation: implications for ethanol steam reforming, *The Journal of Physical Chemistry A*, **114(11)**, 3796–3801 **(2010)**

33. Steele B., Appraisal of $C_{e1-y}G_{dyO2-y/2}$ electrolytes for IT-SOFC operation at 500 °C, *Solid State Ionics*, **129(1–4)**, 95–110 **(2000)**

34. Thangadurai V. and Kopp P., Chemical synthesis of Ca-doped CeO_2-Intermediate temperature oxide ion electrolytes, *Journal of Power Sources*, **168(1 Spec. Iss.)**, 178–183 **(2007)**

35. Tholkappiyan R. and Vishista K., Combustion synthesis of Mg–Er ferrite nanoparticles: Cation distribution and structural, optical and magnetic properties, *Materials Science in Semiconductor Processing*, **40**, 631–642 **(2015)**

36. Tianshu Z., Ionic conductivity in the CeO_2–Gd_2O_3 system ($0.05 \leq Gd/Ce \leq 0.4$) prepared by oxalate coprecipitation, *Solid State Ionics*, **148(3–4)**, 567–573 **(2002)**

37. Venkataswamy P., Jampaiah D., Kandjani A.E., Sabri Y.M., Reddy B.M. and Vithal M., Transition (Mn, Fe) and rare earth (La, Pr) metal doped ceria solid solutions for high performance photocatalysis: Effect of metal doping on catalytic activity, *Research on Chemical Intermediates*, **44(4)**, 2523–2543 **(2018)**

38. Wang B., Zhu B., Yun S., Zhang W., Xia C. and Afzal M., Fast ionic conduction in semiconductor $CeO_{2-\delta}$ electrolyte fuel cells, *NPG Asia Materials*, **11(1)**, 51 **(2019)**

39. Yahiro H., Ohuchi T., Eguchi K. and Arai H., Electrical properties and microstructure in the system ceria-alkaline earth oxide, *J. Mater. Sci*, **23(3)**, 1036–1041 **(1988)**

40. Yamashita K., Ramanujachary K.V. and Greenblatt M., Hydrothermal synthesis and low temperature conduction properties of substituted ceria ceramics, *Solid State Ionics*, **81(1–2)**, 53–60 **(1995)**

41. Zhao K. and Du Y., Calcium-doped ceria materials for anode of solid oxide fuel cells running on methane fuel, *Journal of Power Sources*, **347**, 79–85 **(2017)**

42. Zheng Y., He S., Ge L., Zhou M., Chen H. and Guo L., Effect of Sr on Sm-doped ceria electrolyte, *International Journal of Hydrogen Energy*, **36(8)**, 5128–5135 **(2011)**

43. Zhu B., Liu X., Sun M., Ji S. and Sun J., Calcium doped ceria-based materials for cost-effective intermediate temperature solid oxide fuel cells, *Solid State Sciences*, **5(8)**, 1127–1134 **(2003)**.

(Received 24th August 2021, accepted 25th September 2021)